ICESat-2 Pointing Calibration and Geolocation Performance

S.B. Luthcke[1], T.C. Thomas[2], T.A. Pennington[3], T.W. Rebold[2], J.B. Nicholas[2], D.D. Rowlands[1], A.S. Gardner[4], S. Bae[5]

[1]Geodesy and Geophysics Laboratory, NASA Goddard Space Flight Center, Greenbelt, Maryland, USA

[2]Emergent Space Technologies @ Goddard Space Flight Center, Greenbelt, Maryland, USA

[3]KBRwyle @ Goddard Space Flight Center, Greenbelt, Maryland, USA

[4]Jet Propulsion Laboratory, California Institute of Technology, Pasadena, CA 91109, USA

[5]Applied Research Laboratories, the University of Texas at Austin, Austin, Texas, USA

Corresponding author: Scott B. Luthcke (Scott.B.Luthcke@nasa.gov)

Key Points:

- Systematic time varying pointing errors are the largest ICESat-2 pointing control and geolocation knowledge error source
- The systematic pointing errors have been calibrated and corrected to meet and exceed the mission geolocation requirements
- Further geolocation improvements can be made through the application of the relative beam alignment calibration

Abstract

ICESat-2 science requirements are dependent on the accurate real-time pointing control (i.e. geolocation control) and post-processed geolocation knowledge of the laser altimeter surface returns. Pre-launch pointing alignment errors and post-launch pointing alignment variation result in large geolocation errors that must be calibrated on orbit. In addition, the changing sun-orbit geometry causes thermal-mechanical forced laser frame alignment variations at the orbit period and trends from days, weeks and months. Early mission analysis computed precise post-launch laser beam alignment calibration. The alignment calibration was uploaded to the spacecraft and enabled the pointing control performance to achieve 4.4 ± 6.0 m, a significant improvement over the 45 m (1 σ) mission requirement. Laser frame alignment calibrations are used to reduce the alignment bias and time variation, as well as the orbital variation contributions to geolocation knowledge error from 6 m to 1.7 m (1 σ). Relative beam alignment of the six beams is calibrated and shown to contribute between 0.5 ± 0.1 m and 2.4 ± 0.2 m of remaining geolocation knowledge error. Independent geolocation assessment based on comparison to high-resolution digital elevation models agrees well with the calibration geolocation error estimates. The analysis demonstrates the ICESat-2 mission is performing far better than its geolocation knowledge requirement of 6.5 m (1 σ) after the laser frame alignment bias variation and orbital variation calibrations have been applied. Remaining geolocation error is beam dependent and ranges from 2.5 m for beam 6 to 4.4 m for beam 2 (mean + 1 σ).

1 Introduction

The National Aeronautics and Space Administration (NASA) launched the Ice Cloud and Land Elevation Satellite 2 (ICESat-2) mission on September 15, 2018 to continue satellite laser altimeter observations of Earth's cryosphere (ice sheet, glacier, and sea ice) and vegetation. These measurements were first established by the ICESat mission launched a decade and a half earlier in 2003. The primary mission science requirements for ICESat-2 include quantifying ice sheet surface elevation change to an accuracy better than 0.4 cm/yr annually, measuring outlet glacier (100 km^2 resolution) year-to-year elevation change averages to an accuracy better than 25 cm/yr, determining sea-ice freeboard with an uncertainty less than 3 cm along 25 km segments, and producing elevation measurements that enable independent determination of global vegetation height with ground track spacing of less than 2 km over 2 years (Markus et al., 2017). In order to meet these demanding mission science requirements, ICESat-2 acquires precise surface elevation measurements along a global set of 1387 repeat reference ground tracks (RGTs) in the polar regions, and performs satellite attitude off-RGT pointing of the lasers for improved vegetation mapping in the mid- and low-latitudes. To enable this global RGT sampling, ICESat-2 is in a 92º inclination, ~494 km mean altitude, frozen 91 nodal day (90.8193 days) repeat orbit (Markus et al., 2017).

The ICESat-2 mission's primary instrument is the Advanced Topographic Laser Altimeter System (ATLAS). The ATLAS instrument is a photon counting laser altimeter operating at 532 nm (green) wavelength (Neumann et al., 2019). The laser energy is split into six separate beams by a Diffractive Optical Element (DOE) to optimize surface elevation sampling and to minimize surface elevation change errors from repeat track analysis. The six laser beams are arranged in

three pairs (Markus et al., 2017). Each pair has a strong and weak power beam with 90 m surface (on the Earth) cross-track separation within the pair. The pairs are arranged with 3.3 km surface cross-track separation. Each laser beam has a surface footprint approximately 12 m in diameter. The laser transmits micro-pulses at a 10 kHz repetition rate, which translates into 74 cm along-track sampling for each beam. The ATLAS instrument measures the round-trip (2-way) time of flight, from laser transmit, to surface bounce point, and back to the instrument receiver.

ICESat-2 is designed for precise repeat surface elevation measurements that places tight requirements on pointing control and geolocation knowledge. The precise geolocation measurement model is evaluated in the inertial reference frame using: the ATLAS instrument 2-way range measurement correcting for atmospheric path delay, the laser pointing in the inertial reference frame, and the instrument position in the inertial reference frame (Luthcke et al., 2019a). The inertial bounce point position is then transformed to the Terrestrial Reference Frame (TRF) for final precise geolocation of the surface bounce points. Therefore, the accurate positioning, or geolocation of the surface bounce points, relies not only on the ATLAS instrument measurements, but also on the ICESat-2 Precision Orbit Determination (POD) and Precision Pointing Determination (PPD) solutions. The ICESat-2 POD is obtained from the analysis and reduction of GPS tracking data acquired from redundant RUAG dual frequency receiver and antenna systems, and ranging data to a nine corner-cube Satellite Laser Ranging (SLR) Retro-Reflector (RR) (Luthcke et al., 2019b). The PPD is computed from two SODERN HYDRA star trackers and a Northrup Grumman Scalable Space Inertial Reference Unit (SSIRU), as well as a dedicated Laser Reference System (LRS). The LRS uses a laser side camera to monitor the motion of the lasers, and a stellar side camera to reference the laser motions with respect to the inertial reference frame (Bae et al., 2018). The PPD sensors are mounted to the optical bench to minimize motion with respect to the lasers as to minimize pointing errors. Unfortunately, once on orbit the stellar side of the LRS suffered significant issues that preclude its data from being used in the PPD determination (Neumann et al., 2019).

Even under the most diligent instrument development, sensor measurement array, and processing algorithms, alignment errors and time varying pointing biases will significantly impact the geolocation (Luthcke et al., 2005). ICESat-2 is no exception with its stringent laser surface bounce point horizontal (on the surface) geolocation knowledge requirement of 6.5 m (1 σ) and pre-launch best estimate of 4.9 m (1 σ) (Neumann et al., 2019). In particular, systematic pointing errors and their variation in time are the largest source of geolocation error remaining and must be calibrated while on orbit (Luthcke et al. 2000 and 2005). To relate pointing angle to geolocation error for ICESat-2: 1 arcsecond of pointing error is approximately 2.4 m of geolocation error on the Earth's surface. The pointing errors are dominated by long-term trends (long period variation on the order of weeks to months) and orbital variation (variation with the satellite orbit period) as the time dependent alignment errors are thermal-mechanically driven by sun-orbit geometry (Luthcke et al. 2000, 2002, and 2005). The spacecraft and instrument experience subtle changes in mechanical alignment due to changing thermal gradients. The change in the thermal gradients have two main drivers. The first is a slow change in time, or long-term trends, that is driven by the change in the angle of the sun to the orbit plane known as the β' angle. The second is the change in sunlight over an orbit period, orbit variation, driven by the change in orbit angle, Ω. The orbit angle is the angle between the satellite position vector and the sun vector projected in the orbit plane where 0° is orbit 6 am and 90° is orbit noon. The

orbit angle completes one cycle in the orbit period of 94.35 minutes. The β' angle goes through a complete cycle in 502 days. The β' angle can range from ± 90° but is modulated by the seasonal sun declination angle. At the high β' angles ICESat-2 is in complete sunlight illuminating its side face opposite the radiator. At low β' angles near zero ICESat-2 goes through maximum eclipse periods, and during the sunlight portion of the orbit the sun is illuminating the zenith face of the spacecraft housing the GPS antennas. The changes in β' angle and orbit angle (Ω) drive both long-term variation (502 day cycle period) and orbit variation (94 minute cycle period) in thermal gradients, and therefore changes in mechanical alignment.

For ICESat-2 the changing alignment errors are further exacerbated by the loss of the LRS stellar side. In addition to geolocation knowledge, ICESat-2 has a 45m (1 σ) real-time spacecraft pointing control (or horizontal geolocation control) requirement to place the laser beams along the RGT (nominally the center pair straddling the RGT) (Neumann et al., 2019). This real-time pointing control depends on the on-orbit calibration of the laser pointing with respect to the spacecraft Attitude Control System (ACS) onboard solution. Here we present the calibration of ICESat-2 time varying systematic pointing errors. We quantify the post-calibration geolocation improvements, and the remaining error in both real-time pointing control and post-processed geolocation knowledge, and demonstrate the ICESat-2 geolocation requirements are being met.

2 Calibration Approach

To calibrate and remove the dominant geolocation errors due to time varying systematic pointing errors, ICESat-2 has adopted the Scan Maneuver (SM) and Range Residual Analysis (RRA) calibration approach (Rowlands et al., 1999, Luthcke et al., 2000 and 2002). This approach was successfully implemented by ICESat to achieve mission geolocation requirements despite the loss of the ICESat LRS (Luthcke et al., 2005). The RRA is also capable of calibrating ranging, timing, and positioning biases in addition to pointing (Rowlands et al., 1999). However, position and timing calibration is not necessary for ICESat and ICESat-2 which both utilize

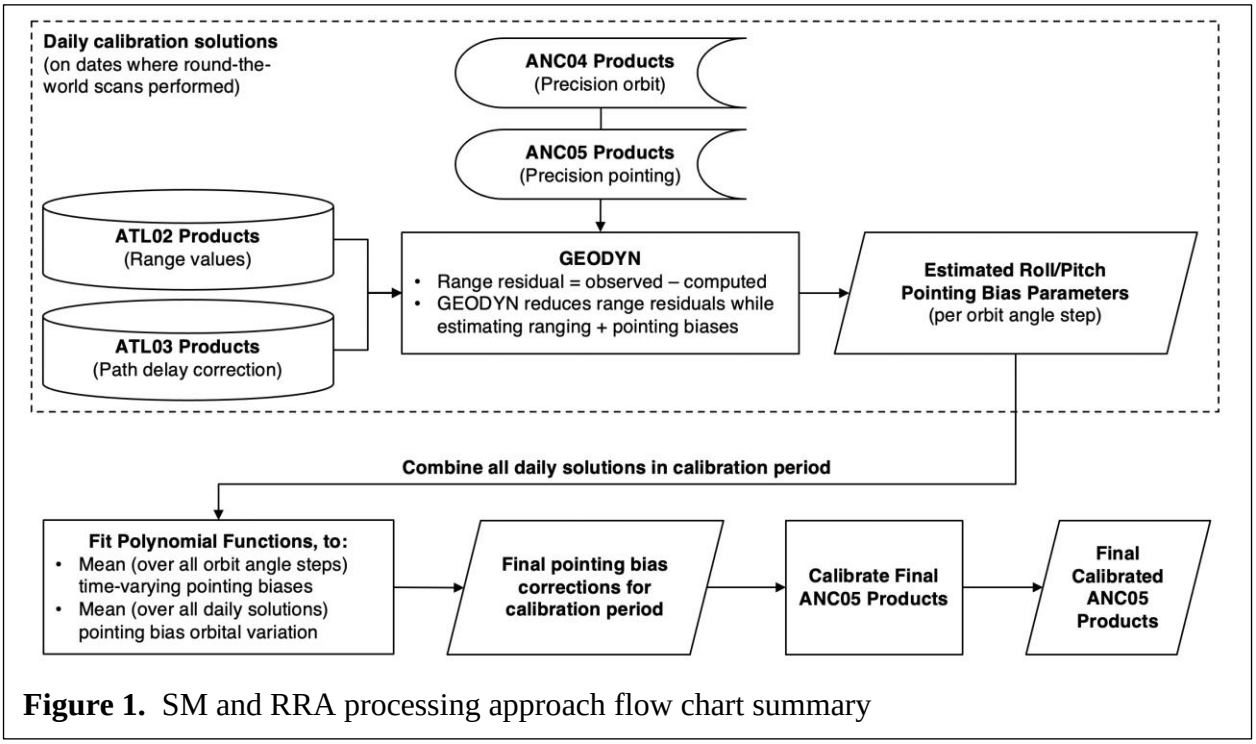

Figure 1. SM and RRA processing approach flow chart summary

precise geodetic GPS receivers for precise positioning and system timing. Figure 1 presents a flow chart summary of the SM and RRA processing approach.

The ICESat-2 range observations are precisely computed in a direct altimetry measurement model. The detailed measurement model computes the round trip range from the satellite to a model of the Earth's surface and back again to the satellite. The position of the transmitted and received tracking points with respect to the satellite's center of mass are modeled. The time dependent variations of the Earth's surface with respect to the Earth's center of mass are also modeled. Many other effects are considered including aberration's effect on pointing (Luthcke et al. 2019a and 2019b). The range residual is the difference between the observed range and computed range. The algorithms are implemented into NASA Goddard Space Flight Center's (GSFC) GEODYN (https://earth.gsfc.nasa.gov/geo/data/geodyn-documentation) precise orbit and geodetic parameter estimation software in order to take advantage of the existing robust estimation scheme and the myriad of model parameters, as well as to combine the altimeter data with other tracking data types.

Estimates of pointing and ranging parameters are obtained from Bayesian least-squares solutions in a batch reduction of the altimeter range residuals. If only nominal science mode range observations are used in these solutions, estimated roll and pitch pointing parameters are very highly correlated. SMs producing observations over the ocean surface are specifically designed to break correlations between these two parameters in batch solutions for calibration parameters. Luthcke et al., 2000 presented a detailed Consider Covariance analysis demonstrating these maneuvers to be a strong filter in isolating the systematic pointing errors and to de-correlate the pointing error components (i.e. roll and pitch) as well as range bias. The analysis also demonstrated errors in the ocean surface model have negligible impact on the recovered pointing parameters unless those errors are very near the maneuver frequency. Therefore, the maneuver period is optimized to minimize the impact from surface modeling error. The SM RRA has the advantage of using global data, and therefore can calibrate orbital variation errors in addition to longer term temporal variation errors. In addition, the SM RRA is independent of ice sheet data used in determining ice sheet surface elevation change.

As with ICESat, the SMs employed by ICESat-2 include ocean scans (OS) and "round"-the-world scans (RTWS). Both SMs consist of small amplitude (1° - 5°) conic-like roll and pitch deviations of the spacecraft attitude from nadir pointing with each individual conic-like maneuver having a period of 10 minutes (Luthcke et al., 2000 and 2005). The OSs are 20-minute SMs consisting of two complete revolutions around the local nadir. The RTWSs consist of multiple 10-minute revolutions continuously performed over the oceans for at least one complete orbit (Figure 2). The OSs sample the same tracks as the RTWSs, but are only 20 minutes long confined to within ± 40° latitude centered on the equator over the pacific ocean**.** For non-interfering RTWSs the spacecraft resumes RGT pointing over the ice sheets and then continues the RTWS over the ocean. The OSs are nominally conducted twice per day on both a mid-Pacific ascending and descending pass. The RTWSs are nominally conducted twice per mission week during the orbit tracks that have long continuous ocean coverage. These RTWSs enable the calibration of systematic pointing error variation as a function of orbit angle (angle between the satellite position vector and the sun vector projected in the orbit plane where for this analysis 0° is orbit 6 am and 90° is orbit noon). Through the reduction of the range residuals from the RTWSs, pointing biases in both the observatory Master Reference Frame (MRF) X and Y axes are nominally estimated every 3.8 minutes or every 15° in orbit angle. The resulting OS and

RTWS calibration history facilitate sub-arcsecond calibration of systematic pointing errors (orientation and amplitude) at time scales of ~ 3.8-minutes to months (Luthcke et al. 2000 and 2005).

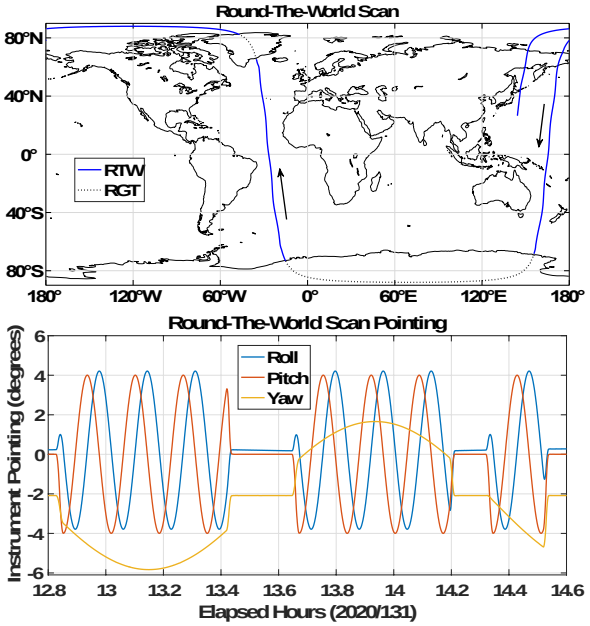

Figure 2. Example of non-interfering ICESat-2 "round"-the-world scans (RTWS). Geographic path of scan maneuver (top), and spacecraft roll and pitch time series (bottom). Time periods where roll and pitch are near zero are during nominal RGT pointing over ice sheets. An Ocean Scan (OS) samples the same ocean tracks as RTWSs, but is limited to 20 minutes confined within ±40° latitude centered on the equator over the pacific ocean**.**

3 Pointing Control Calibration and Performance

ICESat-2 has a stringent pointing control (real-time RGT pointing) requirement of 45 m (1 σ) cross-track. The requirement ensures that the center pair of beams (90 m separation within pair) will straddle the RGTs to minimize surface slope error contribution to the determination of surface elevation change from repeat track analysis. Due to engineering implementation considerations, the spacecraft ACS targets the ATLAS receiver to the RGT and not the laser beams directly. This is a valid approach as the lasers are actively aligned with the receiver in order to collect the reflected ranging photons. However, at launch the spacecraft ACS used pre-launch measured alignment. This alignment was neither measured accurately enough with respect to the ACS solution nor was it assured to remain static through launch. Therefore, ICESat-2 uses the SM RRA to provide the on-orbit ACS alignment of the laser beams needed to meet the mission pointing control requirement.

Early in the mission, after star tracker and ACS configuration setting errors were resolved, it was observed that the total position pointing control error was 1896 m, significantly failing the

mission requirement. RTWSs were then performed to utilize RRA to estimate an alignment correction quaternion (QATLAS2BDY) for upload to the ACS. The first quaternion correction was uploaded on March 28, 2019 and enabled the mission to achieve its pointing control requirement. The last refinement of the quaternion correction was on August 12, 2019 which allowed the mission to far exceed its pointing control mission requirement with performance at 0.1 ± 7.6 m globally. Recent analysis of data on July 14, 2020 shows some temporal drift in the pointing control performance degrading to 4.4 ± 6.0 m globally. Figure 3 presents the pointing control performance showing valid surface return data during RGT pointing. While there has been an alignment drift over the year from initial calibration and upload of the alignment correction quaternion, the performance is far better than the 45 m (1 σ) requirement. Any further drifting and degrading of performance can be corrected with a new upload of the alignment quaternion once performance is deemed unacceptable.

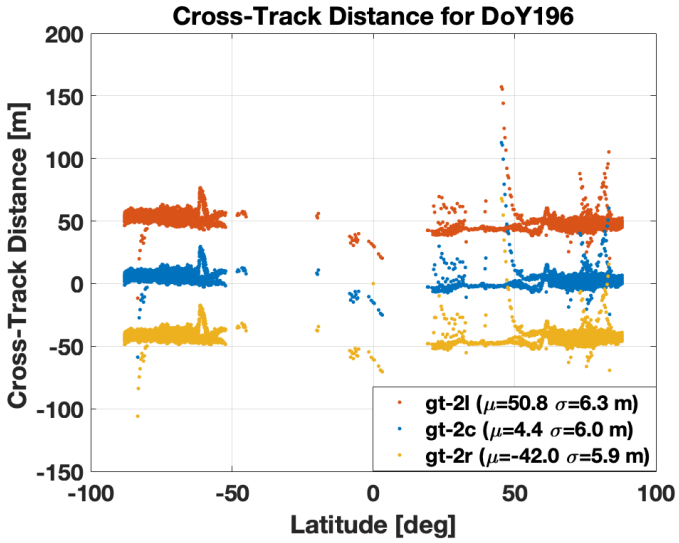

Figure 3. ICESat-2 pointing control performance for a typical day, July 14, 2020, showing valid surface returns from both beams during RGT pointing. Ground track 2 (center pair of beams) left and right (gt-2l and gt-2r) with respect to the RGT in the cross-track direction are shown. gt-2l (orange) and gt-2r (yellow) are separated by 90 m across-track and meant to evenly straddle the RGT (cross-track distance = 0) with both beams being 45 m from the RGT. The center of the pair of beams labeled gt-2c (blue) is computed to show the pointing control performance with respect to the RGT (4.4 ± 6.0 m).

4 Pointing Calibration and Geolocation Knowledge Performance

The accurate geolocation of the ATLAS surface return photons provides the fundamental elevation observations for the ICESat-2 mission to meet its science requirements. The largest geolocation error source for ICESat-2 is the laser pointing alignment biases and variation. Here

we present the calibration of the time variable laser pointing needed to meet the mission post-processed geolocation knowledge requirement.

4.1 Frame Alignment Calibration

The calibrations are first conducted using data from all six beams simultaneously and therefore represent the overall laser frame alignment (common alignment of all beams). The frame alignment errors are the main source of time varying pointing error as the relative beam alignment (alignment between beams) is established by the DOE, and therefore highly stable. Relative alignment biases are computed once the laser frame is calibrated. Pointing biases as a function of orbit angle in both roll (about MRF x-axis) and pitch (about MRF y-axis), along with range biases, are estimated through the reduction of the ocean surface altimeter range residuals from the SMs. Figure 4 presents the pre- and post-calibration altimeter ocean surface range residuals for a typical RTWS. Data gaps in the range residuals are missing surface returns due to cloud cover. Individual calibrations are performed nominally every 3 to 4 days for each day containing an RTWS and include the surrounding OS data from within the 24-hr period. The individual calibrations are then processed in time periods (CAL Periods) to estimate roll and pitch bias trends and mean orbital variation for each CAL Period.

The CAL Periods are irregularly spaced in time as they must be situated with respect to ATLAS Alignment Monitoring and Control System (AMCS) Beam Steering Mechanism (BSM) setpoint changes conducted periodically to co-align the ATLAS laser transmitters and the receiver (Neumann et al., 2019). Through the pointing calibration solution analysis, it has been observed that the AMCS laser pointing changes result in residual laser alignment with respect to the PPD solution, and therefore require the calibration solutions to be positioned with respect to the AMCS changes. In addition, the pointing calibration time periods are aligned with respect to major spacecraft operational orientations and modes, that include sailboat and airplane spacecraft orientation transitions as well as the yaw-flip as these modes represent a change in the thermal mechanical forcings on the instrument. The ICESat-2 observatory is re-oriented with a 180° yaw flip (fly backwards or fly forwards) twice every 502 day β' cycle when the sun transitions through $\beta' = 0°$. The re-orientation is necessary to keep the sun from illuminating the radiator and to optimize sun illumination of the solar array. ICESat-2 further optimizes sun illumination of the array with two solar array modes. When β' is approximately greater than 45° the solar array normal is oriented parallel to the observatory side cross-track face normal (perpendicular to the velocity and nadir vectors) and held fixed as a sail (sailboat mode). When the β' is approximately less than 45° the solar array rotation axis is oriented parallel to the observatory cross-track face normal as an airplane wing (airplane mode) and the array is rotated about its axis once every orbit revolution to track the sun. Figure 5 presents the timeline of CAL Periods with respect to AMCS changes, and major spacecraft mode changes.

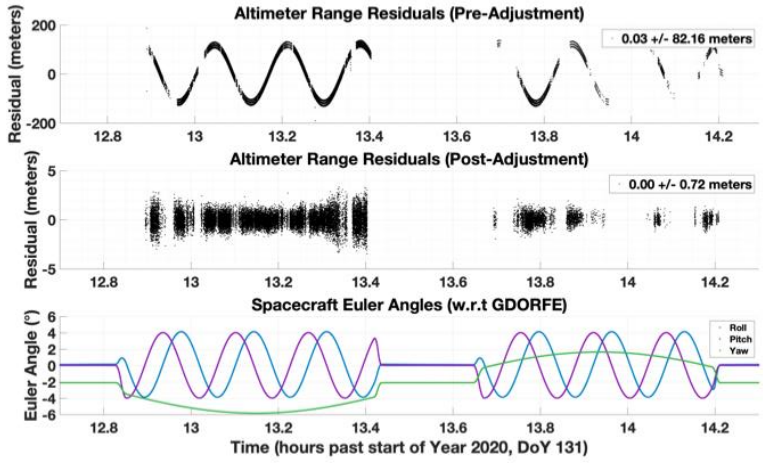

Figure 4. ICESat-2 Pre-calibration altimeter range residuals (top), post-calibration altimeter range residuals (middle), and the spacecraft attitude profile (roll, pitch, yaw) during a RTWS maneuver (bottom). The spacecraft returns to RGT tracking (roll and pitch angles near 0°) while over the ice sheets.

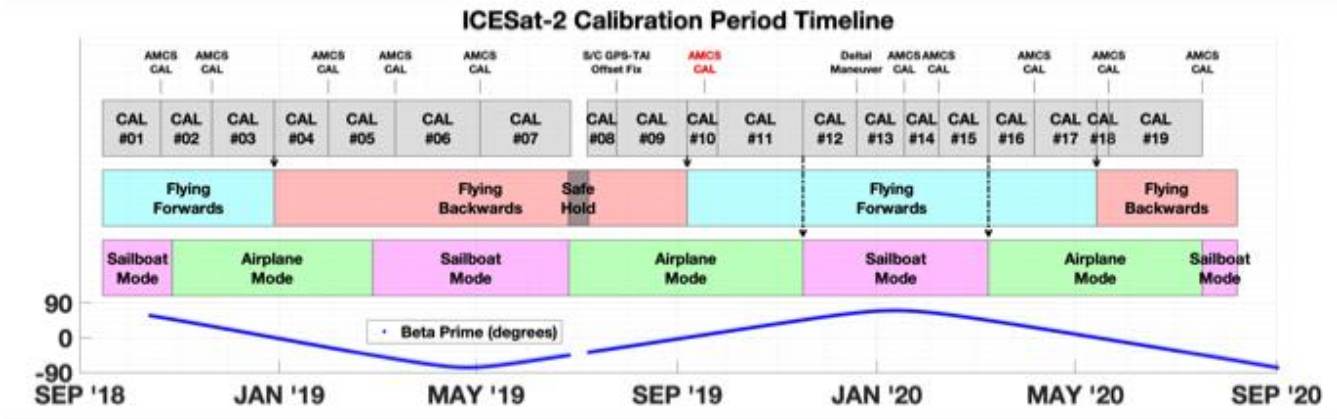

Figure 5. Calibration time periods (CAL Periods) relative to AMCS setpoint changes and spacecraft modes.

The estimated roll and pitch biases within a CAL Period are fit to a function to obtain the pointing bias trend within the CAL Period. The functional fit is chosen as a low degree polynomial to calibrate a portion of the long-term pointing variation caused by the 502 day β'cycle, and to minimize the calibration solution error. For short time periods (~days to a week) there is little change and a simple mean is estimated. For longer time periods (~weeks to months) a linear or quadratic is required to capture the β' cycle forcing. Figure 6 presents an example of the pitch bias trend functions estimated for CAL Periods 17, 18, and 19. The first discontinuity between CAL periods 17 and 18 is due to the spacecraft yaw flip (changing from flying forwards to flying backwards), and the second discontinuity is due to the AMCS setpoint change. The individual calibrated biases are represented by the blue markers and the vertical bars represent the standard deviation of the mean orbit variation for that 24-hr. calibration solution. The impact of the yaw flip causing a thermal-mechanical alignment shift due to the

significant change in spacecraft sun illumination, and the AMCS setpoint change are observed by the significant discontinuities.

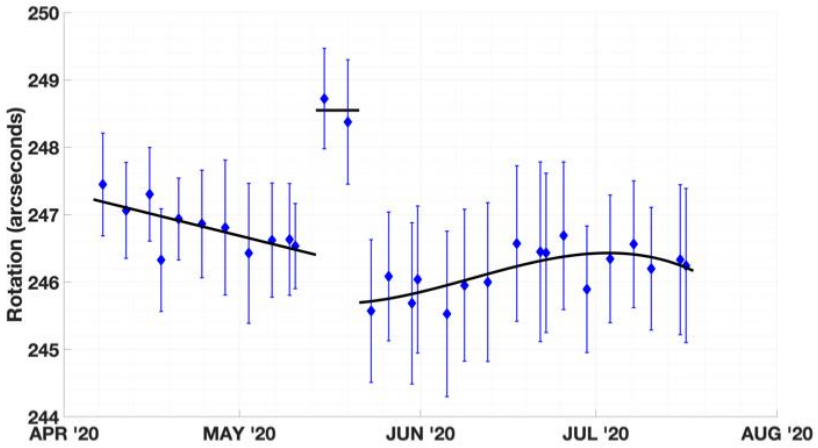

Figure 6. Pitch pointing bias trend calibration for CAL Periods 17 – 19. Blue markers represent individual bias calibrations. Bars represent the standard deviation of the orbit angle variation observed by the individual 24-hr. calibration. The black line is the functional fit of the bias trend. The discontinuities occur at the CAL Period boundaries and are due to the AMCS setpoint changes. 1 arcsecond of pointing error is approximately 2.4 m of geolocation error on the Earth's surface.

The mean orbit variation is then computed through averaging the calibrations within a CAL Period with the roll and pitch biases removed. Figure 7 presents a typical example of the recovered pitch orbit variation for CAL Period 19. The orbit variation is estimated every 15° in orbit angle which represents ~1700 km length track on the Earth's surface. A nearest neighbor covariance constraint is used to condition the orbit angle step solutions that have limited or no ranging data. Orbit variation is typically on the order of 2 to 3 arcseconds peak-to-peak, which represents a geolocation error of approximately 4.8 to 7.2 meters on the ground. A functional fit is used to filter the orbit angle calibration and is the correction applied to calibrate the pointing. A higher degree polynomial (typically 3 – 7) is used to capture the orbit angle (Ω) dependent sun illumination forcing thermal-mechanical pointing variations. The polynomial is constrained to be continuous across the 360° - 0° boundary. The polynomial needs to be of high enough degree to capture the significant pointing shift that is caused when the spacecraft is in an eclipsing period and enters sunlight (Ω = 0°), orbits into maximum sunlight (Ω = 90°), and enters into eclipse (Ω = 180°) (Figure 7).

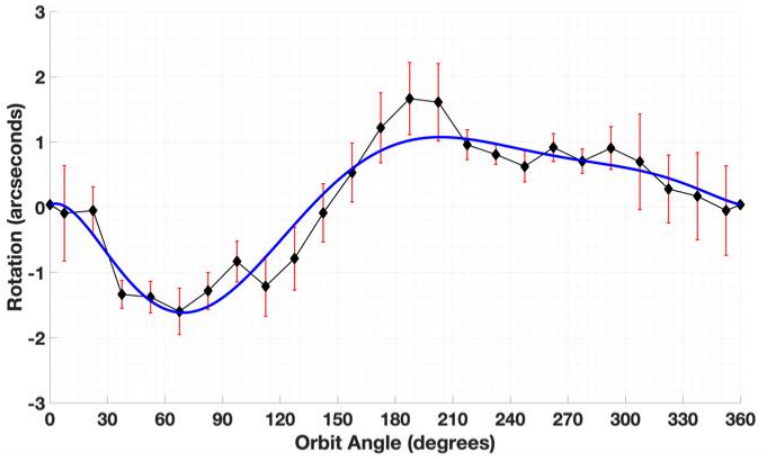

Figure 7. Calibrated pitch orbital variation for CAL Period 19. Orbit angle is the angle between the satellite position vector and the sun vector projected in the orbit plane where for this analysis 0° is orbit 6 am, 90° is orbit noon, 180° is orbit 6 pm, and 270° is orbit midnight. The blue line is the functional fit used to calibrate the pointing. It should be noted the ICESat-2 ANC products have a different orbit angle convention with 0° being midnight.

Once the bias trends and orbital variation are estimated for each CAL Period, the daily PPD solution is then corrected to produce a calibrated PPD solution (calibrated Ancillary PPD, ANC05 product). Figure 8 presents the estimated time varying pointing error pre- and post-calibration for nearly 22 months of the mission covering nearly 1.5 of a beta prime cycle (angle between the sun vector and orbit plane). The markers represent the calibration bias and the bars represent the standard deviation of the orbit variation. Table 1 summarizes the results presented in Figure 8. As expected, the largest error source is the pre-launch static bias that accounts for nearly 1600 m (663 arcseconds total angle) of geolocation error before calibration. Time varying bias for the laser frame alignment and orbit variation account for nearly all of the variance in the geolocation error prior to calibration. Post-calibration the geolocation error contribution from laser frame alignment bias, bias variation and orbit variation has been reduced from 6 m to 1.7 m.

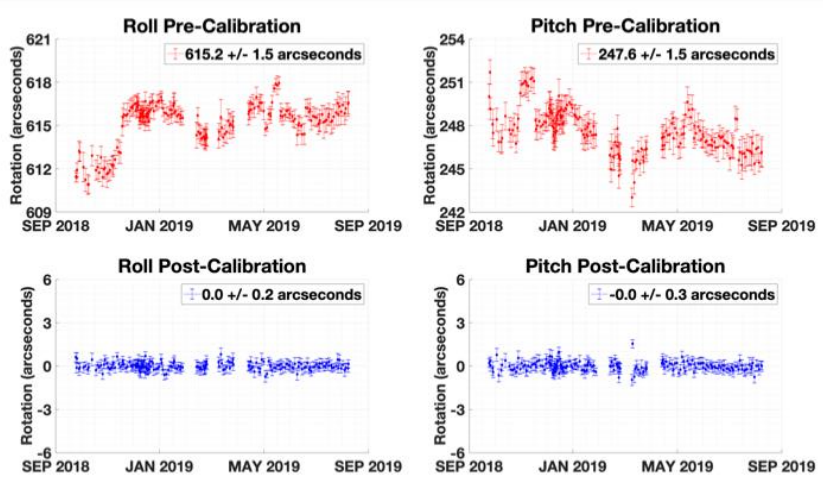

Figure 8. ICESat-2 time varying pointing error pre- and post- calibration and correction. The bars represent the standard deviation of the orbital variation per calibration.

Table 1. Laser Frame Alignment Calibration Summary

	Roll (arcsecond)	Pitch (arcsecond)	Total Geolocation Error (m)
Pre-Calibration			
Mission Bias	615.2	247.6	1591.6
Bias variation (1 σ)	1.5	1.5	5.1
Orbit variation (1 σ)	0.8	1.0	3.1
Bias and Orbit variation (1 σ)	1.7	1.8	6.0
Post-Calibration - Corrected			
Mission Bias	0.0	0.0	0.0
Bias variation (1 σ)	0.2	0.3	0.9
Orbit variation (1 σ)	0.4	0.4	1.4
Bias and Orbit variation (1 σ)	0.5	0.5	1.7

4.2 Relative Beam Alignment

The relative beam alignment is then calibrated from 187 calibrations (days) from SM and RRA using the PPD solutions corrected for the laser frame alignment calibrations discussed in section 4.1. Table 2 summarizes the relative beam alignment calibration results. The mean and standard error of the mean are presented for each beam relative to the corrected laser frame.

Table 2. Relative Beam Alignment Calibration Summary (mean ± standard error from 187 (days) calibrations)

Beam Number	Roll mean (arcsecond)	Pitch mean (arcsecond)	Geolocation Error mean (m)
1 - Strong	+0.5 ± 0.04	+0.6 ± 0.05	1.9 ± 0.2
2 - Weak	+1.0 ± 0.04	+0.1 ± 0.04	2.4 ± 0.2
3 - Strong	-0.3 ± 0.03	-0.5 ± 0.04	1.4 ± 0.1
4 - Weak	+0.2 ± 0.04	+0.5 ± 0.04	1.3 ± 0.1
5 - Strong	-0.5 ± 0.03	-0.3 ± 0.03	1.4 ± 0.1
6 - Weak	+0.0 ± 0.04	-0.2 ± 0.04	0.5 ± 0.1

4.3 Total Pointing and Geolocation Error

At the time of writing, the ICESat-2 pointing solutions (as of data release 3) have been corrected for the laser frame alignment calibration presented in section 4.1, but have not yet been corrected for the relative beam alignment calibrations presented in section 4.2. Table 3 summarizes the current total pointing error (root sum square (RSS) of roll and pitch) combining the remaining post-calibration laser frame alignment bias and orbit variation error (Table 1), and the relative beam alignment error (Table 2). In addition to these longer wavelength error sources (3.8 minutes or 1700 km and longer), we have included the current 0.4 arcsecond (1 σ) estimate of the PPD solution error which represents the short wavelength errors. The pointing calibration results presented in Table 3 demonstrate that all beams are now (as of data release 3) well within the mission geolocation requirement of 6.5 m post laser frame calibration and correction. Beams 1 and 2 are the poorest performing with beam 2 having nearly all of its 2.4 m bias in the cross-track (roll) direction.

Table 3. Total Pointing and Geolocation Error (includes post-calibration laser frame alignment errors, relative beam alignment errors, and 0.4 arcsecond 1 σ PPD solution error).

Beam Number	RSS roll and pitch mean ± 1 σ (arcsecond)	Geolocation Error mean ± 1 σ (m)	Total Geolocation Error mean + 1 σ (m)
1 - Strong	0.8 ± 0.8	1.9 ± 2.0	3.9
2 - Weak	1.0 ± 0.8	2.4 ± 2.0	4.4
3 - Strong	0.6 ± 0.8	1.4 ± 2.0	3.4
4 - Weak	0.5 ± 0.8	1.3 ± 2.0	3.3
5 - Strong	0.6 ± 0.8	1.4 ± 2.0	3.4
6 - Weak	0.2 ± 0.8	0.5 ± 2.0	2.5

5 Independent Validation

As an independent geolocation assessment, we employ a trigonometric relationship between ICESat-2 elevation residuals with a reference Digital Elevation Model (DEM) and the local DEM slope and aspect to determine ICESat-2 track offsets (Nuth and Kaab, 2011). The analysis is performed using ICESat-2 Region 3 and 5 granules which extend from 59.5° to 80° north latitude. Region 3 represents ascending tracks and Region 5 is descending. These granules are chosen as they sample sufficient surface relief to reliably estimate the across and along-track offsets. The track offsets are computed from the ArcticDEM 10m mosaic (Porter et al., 2018). The solutions are sampled in 6-day intervals where the median of all the track offsets within the interval is computed and used as that discrete interval solution. Intervals with a low number of track solutions are excluded from the analysis.

Table 4 summarizes the estimated geolocation error from the track offset analysis. The magnitudes of the track offsets are summarized to compare with the geolocation error computed from the pointing calibrations presented in Tables 2 and 3. We summarize the track offset magnitudes without considering direction (sign), because a constant pointing bias translates into a track offset geolocation error that will have an opposite sign on either side of the yaw flip (flying backwards vs. forwards), and therefore would cancel. Comparison of the geolocation error estimates from the calibrations in Table 3 and the independent DEM comparisons in Table 4 show good agreement with the worst comparison at 0.6 m. The sub-meter differences can be expected as the DEM comparisons are from a limited latitude band sampling, while the calibrations represent a global sampling. The DEM comparisons show larger mean total error and smaller 1 σ variation than the calibration estimates, which is also to be expected as the DEM estimates are from a 20.5° latitude band. The sampling from the 20.5° latitude band corresponds to a little over one of the 15° steps in the orbit variation calibration, and therefore impart the orbital calibration step value to the mean and no contribution to the 1 σ variation. Both the calibrations and the DEM estimates show the mission geolocation is performing significantly better than the 6.5 m geolocation knowledge requirement. Both the calibration results and the

DEM results show good agreement concerning the relative beam geolocation performance as both show the worst performing beam is beam 2 followed by beam 1, and the best performing is beam 6. In addition, both geolocation assessments show that the largest error component is beam 2 mean in the cross-track (roll) direction (Table 2 vs. Table 4). Both geolocation assessments show the beam 2 anomaly is due to the mean offset and not the standard deviation. Therefore, the increased error is not caused by larger time variation. The larger error is in the overall mean, and therefore a mean alignment error. This could be due to an error anomaly in the pre-launch alignment characterization or could indicate receiver shadowing of the return energy. Further analysis and investigation are needed to isolate the cause.

Table 4. Geolocation Error Estimate from ArcticDEM 10m Comparison

Beam Number	Cross-track Magnitude Region 3+5 mean ± 1 σ (m)	Along-track Magnitude Region 3+5 mean ± 1 σ (m)	Geolocation Error Region 3+5 mean ± 1 σ (m)	Total Geolocation Error Region 3+5 mean + 1 σ (m)
1 - Strong	1.5 ± 1.1	1.8 ± 1.4	2.4 ± 1.8	4.2
2 - Weak	2.8 ± 1.3	1.6 ± 1.0	3.2 ± 1.6	4.8
3 - Strong	1.0 ± 0.8	1.4 ± 0.8	1.7 ± 1.1	2.8
4 - Weak	1.3 ± 1.0	1.3 ± 1.1	1.8 ± 1.5	3.3
5 - Strong	1.2 ± 0.8	1.2 ± 0.7	1.7 ± 1.1	2.8
6 - Weak	0.9 ± 0.7	1.2 ± 0.7	1.5 ± 1.0	2.5

6 Conclusions

ICESat-2 fundamental science requirements are dependent on the accurate real-time pointing control and post-processed geolocation knowledge of the altimeter laser surface returns. The largest error source precluding ICESat-2 from meeting its geolocation requirements is the laser beam pointing. Pre-launch alignment measurement errors and post-launch alignment shifts induce large pointing errors that must be calibrated on orbit. In addition, the changing sun-orbit geometry causes thermal-mechanical forced laser frame alignment variations at the orbit period and trends from days, weeks and months. These alignment biases and variations are calibrated using specifically designed calibration maneuvers and range residual analysis.

The post-launch alignment biases accounted for over 1500 m of pointing control and knowledge error. Early mission SM calibrations provided correction quaternions that were uploaded to the spacecraft to achieve and perform far better than the mission pointing control requirement of 45 m (1 σ). Current pointing control performance is 4.4 ± 6.0 m, and can be further improved if necessary with a more recent alignment calibration upload. Uncorrected laser frame alignment bias variation and orbital variation account for 6 m (1 σ) of geolocation knowledge error, nearly all of the 6.5 m requirement. AMCS setpoint changes have been observed to cause pointing bias

discontinuities, and therefore the calibration periods are arranged and aligned with AMCS and spacecraft mode changes.

Laser frame alignment errors have been calibrated over 22 months of the mission, nearly 1.5 times the sun-orbit cycle period (beta prime period). The laser frame alignment calibrations are used to correct the pointing solution and to reduce the alignment bias variation and orbital variation contribution to geolocation error from 6 m to 1.7 m (1 σ). Relative beam alignment error is calibrated and shown to contribute between 0.5 ± 0.1 m and 2.4 ± 0.2 m of error and is beam dependent. The relative beam alignment calibrations are not yet used (as of data release 3) to correct the pointing solutions, and are therefore currently the largest source of geolocation error. The total geolocation error is beam dependent and ranges from 2.5 m to 4.4 m. Independent DEM geolocation error estimates from a 20.5° latitude band (59.5° to 80°) range from 2.5 to 4.8 m. Both geolocation error assessments show good agreement concerning the relative beam geolocation performance as both show the worst performing beam is beam 2 followed by beam 1, and the best performing is beam 6. The results show that the overall geolocation performance of data release 3 is far better than the 6.5 m (1 σ) requirement.

Geolocation improvements will be realized in future data releases through the application of the relative beam alignment calibrations to further correct pointing errors. This is expected to improve geolocation performance to approximately 2 m with improved consistency across the beams. In addition, calibration improvements including the combination of dynamic cross-over data with the SM data will provide improved resolution of orbital variation and will allow for the calibration of range bias at the sub-cm level (Rowlands et al., 1999, and Luthcke et al., 2005).

Acknowledgments

The specific ICESat-2 datasets used for this research are available at the NASA Distributed Active Archive Center (DAAC) at the National Snow and Ice Data Center (NSIDC). Specifically, the following datasets were used:

> The ATLAS/ICESat-2 L1B Converted Telemetry Data, Version 3, ATL02 data product, https://nsidc.org/data/ATL02/versions/3, global data granules for the time period September 2018 through August 2020 (Martino et al., 2020).
>
> The ATLAS/ICESat-2 L2A Global Geolocated Photon Data, Version 3, ATL03 data product, https://nsidc.org/data/ATL03/versions/3, global data granules for the time period September 2018 through August 2020 (Neumann et al., 2020).

DEMs provided by the Polar Geospatial Center under NSF-OPP awards 1043681, 1559691, and 1542736.

> 10 m ArcticDEM Mosaic data files used in this research are available at the following: http://data.pgc.umn.edu/elev/dem/setsm/ArcticDEM/mosaic/v3.0/10m/. All sub-tile files were used (Porter et al., 2018).

The authors would like to acknowledge Xu Yang (KBRwyle) and Aseel Syed (Emergent Space Technologies) for their data analysis support. The authors would also like to acknowledge Despina Pavlis (UMD) for her many years of dedicated GEODYN maintenance support.

References

Bae, S., Magruder, L., Smith, N., and Schutz, B. (2018), ICESat-2 Algorithm Theoretical Basis Document for Precision Pointing Determination Version 2.0, ICESat-2-SIPS-SPEC-1595

Luthcke, S.B., Rowlands, D.D., McCarthy, J.J., Stoneking, E. and Pavlis, D.E. (2000), Spaceborne Laser Altimeter Pointing Bias Calibration From Range Residual Analysis, *Journal of Spacecraft and Rockets, 37(3),* 374-384, doi:10.2514/2.3571

Luthcke, S.B., Carabajal, C.C and D.D. Rowlands (2002), Enhanced Geolocation of Spaceborne Laser Altimeter Surface Returns: Parameter Calibration from the Simultaneous Reduction of Altimeter Range and Navigation Tracking data, *Journal of Geodynamics, 34(3-4),* 447-475, doi:10.1016/S0264-3707(02)00047-9

Luthcke, S.B., D.D. Rowlands, T.A. Williams, M. Sirota (2005), Calibration and reduction of ICESat geolocation errors and the impact on ice sheet elevation change detection," *Geophys. Res. Lett., 32(21),* doi:10.1029/2005GL023689

Luthcke, S., Pennington, T., Rebold, T., Thomas, T. (2019a), ICESat-2 Algorithm Theoretical Basis Document for ATL03g ICESat-2 Receive Photon Geolocation Version 6.0, ICESat-2-SIPS-SPEC-0142

Luthcke, S., Pennington, T., Rebold, T., Thomas, T. (2019b), ICESat-2 Algorithm Theoretical Basis Document for Precision Orbit Determination and Geolocation Parameter Calibration Version 2.0, ICESat-2-SIPS-SPEC-0140

Markus, T., Neumann, T., Martino, A., Abdalati, W., Brunt, K., Csatho, B., Farrell, S., Fricker, H., Gardner, A., Harding, D., Jasinski, M., Kwok, R., Magruder, L., Lubin, D., Luthcke, S., Morison, J., Nelson, R., Neuenschwander, A., Palm, S., Popescu, S., Shum, C.K., Schutz, B.E., Smith, B., Yang, Y., Zwally, H.J. (2017), The Ice, Cloud and land Elevation Satellite-2 (ICESat-2): Science Requirements, Concept, and Implementation. *Remote Sensing of the Environment*, 190, 260-273. doi: 10.1016/j.rse.2016.12.029

Martino, A. J., M. R. Bock, C. Gosmeyer, C. Field, T. A. Neumann, D. Hancock, R. L. Jones III, P. W. Dabney, C. E. Webb, and J. Lee. 2020. *ATLAS/ICESat-2 L1B Converted Telemetry Data, Version 3*. [Global data, Sept. 2018 through August 2020]. Boulder, Colorado USA. NASA National Snow and Ice Data Center Distributed Active Archive Center. doi: https://doi.org/10.5067/ATLAS/ATL02.003. [Date Accessed].

Neumann, T., Martino, A., Markus, T., Bae, S., Bock, M., Brenner, A., Brunt, K., Cavanaugh, J., Fernandes, S., Hancock, D., Harbeck, K., Lee, J., Kurtz, N., Luers, P., Luthcke, S., Magruder, L., Pennington, T., Ramos-Izquierdo, L., Rebold, T., Skoog, J., Thomas, T. (2019), The Ice, Cloud, and Land Elevation Satellite – 2 Mission: A Global Geolocated Photon Product Derived From the Advanced Topographic Laser Altimeter System, *Remote Sensing of Environment*, 233, doi:10.1016/j.rse.2019.111325

Neumann, T. A., A. Brenner, D. Hancock, J. Robbins, J. Saba, K. Harbeck, A. Gibbons, J. Lee, S. B. Luthcke, T. Rebold, et al. (2020), *ATLAS/ICESat-2 L2A Global Geolocated Photon Data, Version 3*. [Global data, Sept. 2018 through August 2020]. Boulder, Colorado USA. NASA National Snow and Ice Data Center Distributed Active Archive Center. doi: https://doi.org/10.5067/ATLAS/ATL03.003. [Date Accessed].

Nuth, C. & Kääb, Andreas. (2011). Co-registration and bias corrections of satellite elevation data sets for quantifying glacier thickness change. The Cryosphere, 5(1), 271-290. 10.5194/tc-5-271-2011

Porter, Claire; Morin, Paul; Howat, Ian; Noh, Myoung-Jon; Bates, Brian; Peterman, Kenneth; Keesey, Scott; Schlenk, Matthew; Gardiner, Judith; Tomko, Karen; Willis, Michael; Kelleher, Cole; Cloutier, Michael; Husby, Eric; Foga, Steven; Nakamura, Hitomi; Platson, Melisa; Wethington, Michael, Jr.; Williamson, Cathleen; Bauer, Gregory; Enos, Jeremy; Arnold, Galen; Kramer, William; Becker, Peter; Doshi, Abhijit; D'Souza, Cristelle; Cummens, Pat; Laurier, Fabien; Bojesen, Mikkel (2018), "ArcticDEM", https://doi.org/10.7910/DVN/OHHUKH, Harvard Dataverse, V1. [Date Accessed].

Rowlands, D.D., D.E. Pavlis, F.G. Lemoine, G.A. Neuman and S.B. Luthcke (1999), The use of laser altimetry in the orbit and attitude determination of mars global surveyor, Geophysical Research Letters, 26(9), 1191-1194. 10.1029/1999GL900223

Acronyms

ACS	Attitude Control System
AMCS	Alignment Monitoring and Control System
ANC	Ancillary data products
ATLAS	Advanced Topographic Laser Altimeter System
BSM	Beam Steering Mechanism
CAL	Calibration time period
DEM	Digital Elevation Model
DOE	Diffractive Optical Element
GEODYN	NASA GSFC POD and Geodetic Parameter Estimation Software
GSFC	Goddard Space Flight Center
ICESat	Ice Cloud and Land Elevation Satellite
ICESat-2	Ice Cloud and Land Elevation Satellite 2
LRS	Laser Reference System
MRF	Master Reference Frame
OS	Ocean Scan
POD	Precision Orbit Determination
PPD	Precision Pointing Determination
RGT	Reference Ground Track
RR	Retro-Reflector
RRA	Range Residual Analysis
RSS	Root Sum Square
RTWS	“Round” The World Scan
SLR	Satellite Laser Ranging
SM	Scan Maneuver

SSIRU	Scalable Space Inertial Reference Unit
TRF	Terrestrial Reference Frame
UTC	Universal Time Coordinated